Materials Research Express

PAPER

Analysis of superconducting response and flux pinning ability of $(Mg_{0.8}Zn_{0.2}Fe_2O_4)_x$/CuTl-1223 composites

To cite this article: Irfan Qasim *et al* 2019 *Mater. Res. Express* **6** 046002

Materials Research Express

PAPER

Analysis of superconducting response and flux pinning ability of $(Mg_{0.8}Zn_{0.2}Fe_2O_4)_x$/CuTl-1223 composites

Irfan Qasim[1], **Owais Ahmad**[1], **Muhammad Farooq Nasir**[1], **Muhammad Imran Malik**[2], **Qurat ul Ain Javed**[2], **Nawazish A Khan**[3], **Asad Raza**[3], **Muhammad Mumtaz**[4] and **Muhammad Rashid**[5]

[1] Materials Science Laboratory, Department of Physics FEAS, Riphah International University (RIU) Islamabad 44000, Pakistan
[2] School of Electrical Engineering and Computer Science, National University of Sciences and Technology (NUST) Islamabad 44000, Pakistan
[3] Materials Science Laboratory, Department of Physics, Quaid-i-Azam University (QAU) Islamabad 44000, Pakistan
[4] Materials Research Laboratory, Department of Physics FBAS, International Islamic University (IIU) Islamabad 44000, Pakistan
[5] Department of Physics, COMSATS University, Islamabad 44000, Pakistan

E-mail: dr.irfanqasim@gmail.com

RECEIVED
13 December 2018

REVISED
26 December 2018

ACCEPTED FOR PUBLICATION
7 January 2019

PUBLISHED
23 January 2019

Keywords: $(Mg_{0.8}Zn_{0.2}Fe_2O_4)_x$/CuTl-1223 nano-superconductor composites, flux pinning, superconducting volume fraction, activation energy, sol-gel method

Abstract

The superconducting properties of $(Mg_{0.8}Zn_{0.2}Fe_2O_4)_x/Cu_{0.5}Tl_{0.5}$–1223 matrix for concentrations (x = 0.0, 0.5, 1.0, 1.5 wt%) were synthesized by two-step solid state reaction method and analyzed by different characterization techniques. The magnetic $Mg_{0.8}Zn_{0.2}Fe_2O_4$ nanoparticles were synthesized by sol-gel technique separately and later inserted in CuTl-1223 superconducting matrix to obtain final product. The $Mg_{0.8}Zn_{0.2}Fe_2O_4$ nanoparticles were separately characterized by various techniques such as x-ray Diffraction, Scanning Electron Microscopy (SEM), Energy Dispersive x-ray Spectroscopy (EDX) and Vibrating Sample Magnetometer (VSM). The superconducting $(Mg_{0.8}Zn_{0.2}Fe_2O_4)_x$/CuTl-1223 composite samples (x = 0 ∼ 1.5 wt%) were also characterized by various available characterization techniques. The XRD analysis showed spinel cubic structures of magnetic nanoparticles and tetragonal structure of superconducting composites. The XRD spectra revealed that the tetragonal structure of CuTl-1223 superconducting phase was not disturbed after the inclusion of magnetic $Mg_{0.8}Zn_{0.2}Fe_2O_4$ nanoparticles. The behavior of $Mg_{0.8}Zn_{0.2}Fe_2O_4$ was found ferromagnetic in nature during an applied magnetic field. The FTIR analysis exhibited results that $Mg_{0.8}Zn_{0.2}Fe_2O_4$ nanoparticles are settled at grain-boundaries and there is no major variation in oxygen modes. The value of critical temperature $T_c(0)$ reduce with increase in magnetic nanoparticles content. The reduction in activation energy is also noticed with greater addition of magnetic nanoparticles. The overall suppression of critical parameters and activation energy values is due to the net spin of ferromagnetic natured $Mg_{0.8}Zn_{0.2}Fe_2O_4$ nanoparticles, which may scatter charge carriers and increase dissipation energy and ultimately result in pair breaking and resistive broadening to deteriorate flux pinning ability of the superconducting composite matrices.

Introduction

Superconducting volume fraction and Intergrains coupling are two essential parameters in order to develop the critical parameters of high temperature superconductors (HTSCs). CuTl-1223 is considered as a best superconductor because of its high critical parameters, least superconducting anisotropy and long coherence length. The general series of this family is specified as $(Cu_{0.5}Tl_{0.5}Ba_2Ca_{n-1}Cu_nO_{2n+4-\delta}$ [CuTl-12(n − 1)n]; n = 2, 3, 4). The superconducting properties of CuTl-1223 are affected due to intergrain voids, pores and cracks. In superconductors, the main problem is the motion of vortices. The motion of vortices can be pinned and flux pinning strength can be improved inside the superconductors by introducing artificial pinning centers. In literature, various techniques such as chemical doping, ion irradiation and additives have been used in this

aspect. But the most effective technique is the inclusion of nanostructures in the form of nanoparticles, nanorods and nanowires in the host superconducting material. The inclusion of nanoparticles in host superconductors is still preferred in many of the available high temperature superconducting (HTSC's) families for the enhancement of critical parameters. The inclusion of ZnO and ZrO_2 nanoparticles in Gd-123 matrix has enhanced its critical parameters (T_c, J_c and H_c) [1, 2]. The inclusion of $Co_{0.5}Ni_{0.5}Fe_2O_4$ and Co_3O_4 nanoparticles in Bi-2223 phase has enhanced the critical current density J_c [3, 4]. The addition of Cr_2O_3 nanoparticles in (Bi, Pb)-2223 superconductor has improved its superconducting parameters up to $x \leqslant 0.5$ wt% [5]. The inclusion of $CoFe_2O_4$ nanoparticles in $GdBa_2Cu_3O_{7-\delta}$ superconductor has improved its critical parameters like T_c and J_c upto an optimized level of concentration of nanoparticles ($x = 0.01$ wt%). This proved the increase of flux pinning in $GdBa_2Cu_3O_{7-\delta}$ superconductor. Similarly, enhancement of critical parameters and flux pinning were observed after the addition of $(Fe_2O_3)_x(CeO_2)_{1-x}$ and $BaTiO_3$ nanoparticles in $YBa_2Cu_3O_{7-\delta}$ superconductor [6, 7]. Improvement of the superconducting volume fraction and the reduction in porosity of CuTl-1223 phase were reported after the inclusion of Fe_2O_3, SnO_2 and In_2O_3 nanoparticles in the host superconducting matrix [8, 9]. The superconducting state of CuTl-1223 phase decreases after the addition of $ZnFe_2O_4$ nanoparticles which is due to the paramagnetic nature of $ZnFe_2O_4$ nanoparticles [10]. The inclusion of Y_2O_3 nanoparticles in $Bi_{1.6}Pb_{0.4}Sr_2CaCu_2O_y$ has improved its superconducting properties upto 0.7 wt% [11]. The critical current density J_c was enhanced in the presence of applied magnetic field after adding Al_2O_3 nanoparticles in $YBa_2Cu_3O_x$ superconductor [12]. The transport properties were observed to be improved in (Bi, Pb)-2223 matrix after the injection of Al_2O_3 nanoparticles. The inclusion of Al_2O_3 nanoparticles did not alter the crystalline structure of (Bi, Pb)-2223 [13]. Caixuan Xu studied the superconducting properties of $GdBa_2Cu_3O_{7-\delta}$ by adding BaO_2 and $Gd_2BaCuO_{7-\delta}$ nanoparticles. The addition of BaO_2 nanoparticles (0.1 wt%) repressed the Gd/Ba substitution and therefore increases the'J_c' and 'B_{irr}'values. The J_c value is further improved by the inclusion of fine Gd-211 nanoparticles in the presence of small magnetic field. At $T = 77$ K, J_c value becomes maximum i.e. 86000 A cm^{-2} in the absence of magnetic field [14]. Zouaoui studied the inclusion of Al_2O_3 nanoparticles in (Bi, Pb)$_2Sr_2Cu_3O_x$ sample. $(Al_2O_3)_x$/ (Bi, Pb)$Sr_2Cu_3O_x$ ($x = 0$ and 0.2 wt%) was placed in a magnetic field (0 to 250mT). The magneto resistivity and activation energy of the sample ($x = 0$ and 0.2 wt%) were measured and matched with thermally activated flux flow (TAFF) model. The activation energy U_o of pure sample was found smaller than U_o for $x = 0.2$ wt% sample. In vortex phase figure, the T_g and T_p values were enhanced by adding Al_2O_3 nanoparticles upto 0.2 wt% [15]. The crystal structure and superconducting transport properties of $(CNTs)_x/(YBa_2Cu_3O_7)$were studied by S.Dadras. After XRD, structure was found orthorhombic for $x > 0$ and $x = 0$. All samples were placed in Magnetic field ($0.1 \leqslant H \leqslant 9$ T) one by one to measure V-I values for studying J_c and pinning energy U_j at fixed temperature. The T_c values for all samples were found same while J_c and U_j values were improved by the inclusion of CNTs nanoparticles upto 0.7 wt%. The J_c value for pure sample was 10 times smaller than $(CNTs)_x/(YBa_2Cu_3O_7)$ with $x = 0.7$ wt% [16]. Qurat-ul-ain investigated the superconducting properties of $Cu_{0.5}Tl_{0.5}Ba_2Ca_{2-x}Mn_xCu_3O_{10-\delta}$ with different concentrations ($x = 0, 0.1, 0.15$ wt%). The electrical resistivity was calculated as a function of temperature. The doping of Mn nanoparticles in $Cu_{0.5}Tl_{0.5}Ba_2Ca_{2-x}Mn_xCu_3O_{10-\delta}$ was studied by carrying out fluctuation induced conductivity analysis of conductivity data of samples by Lawrence-Doniach and Aslamazov–Larkin models. The doping of Mn at Cu sites enhanced the width of 2D and 3D conductivity regimes. The coherence length 'ξ' and inter-layer coupling were improved by doping Mn at CuO_2 planer sites. The doping of Mn nanoparticles reduced the $J_c(0)$, $B_{c0}(T)$ and $B_{c1}(T)$ parameters [17].

In the current research we have targeted to analyze the effects of $Mg_{0.8}Zn_{0.2}Fe_2O_4$ ferromagnetic nanoparticles on the superconducting parameters of CuTl-1223 phase. The flux pinning ability of these nanoparticles has been reported. The structure of $Mg_{0.8}Zn_{0.2}Fe_2O_4$ nanoparticles are spinel cubic and show ferromagnetic behavior in nature when placed in an external magnetic field. The net spin associated with the ferromagnetic added nanoparticles can significantly influence the pinning ability and superconducting response of 1223 Phase of CuTl-based family.

Experimental

We prepared our precursor through the solid state reaction method. We took three different compounds such as $Ba(NO_3)_2$, $Ca(NO_3)_2$ and $Cu_2(CN)_2$. All these compounds were mixed in a proper amount. The mixture was put in mortar and grinded for 2 h with the help of pestle. The powered sample was then put in the quartz boat. The quartz boat was placed in the middle of the furnace through an iron rod. The powered sample was fired in a furnace at 860 °C for 24 h. After this, the sample was cooled in the furnace to room temperature. The sample was taken out of the furnace and again grinded in mortar for 1 h. The same process was repeated under the same conditions to obtain our precursor [18]. At 2nd phase we prepared $Mg_xZn_{1-x}Fe_2O_4$ nanoparticles by sol-gel technique. We take the concentration of hydrated magnesium nitrate $Mg(NO_3)_2.6H_2O$, 4.28 g, hydrated zinc

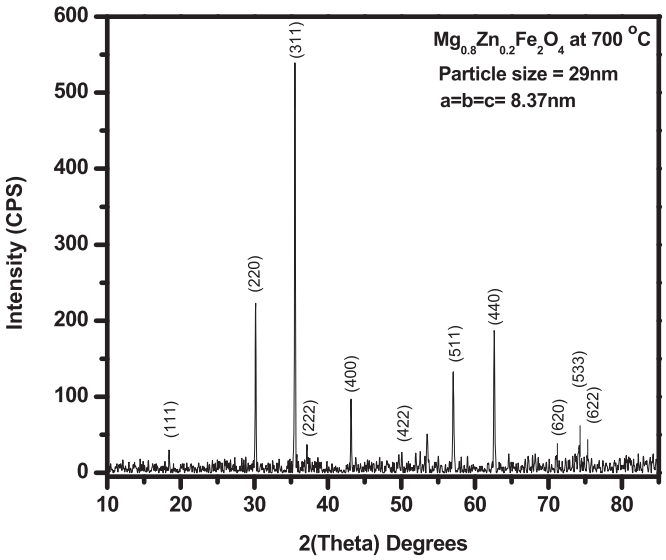

Figure 1. XRD pattern of $Mg_{0.8}Zn_{0.2}Fe_2O_4$ nanoparticles.

nitrate $Zn(N_2O_6).6H_2O$, 1.24 g, iron nitrate $Fe(NO_3)_3$, 14.5 g and citric acid $C_6H_8O_7$. These compounds were mixed and dissolved in distilled water (1 g/10 ml) through constant stirring with the help of a magnetic stirrer. The pH of the solution was checked through a pH meter. The solution was then heated at 70 °C through constant stirring. It took 9 h in the preparation of gel. The gel was then cooled in the air to room temperature. After the formation of gel, it was then dried in the oven for 1 h at 300 °C to remove water molecules and other unwanted impurities. The dried sample was cooled in the oven to room temperature. The dried sample was put in mortar and grinded with the help of pestle until powder is formed. After grinding, the powdered sample was put in quartz boats for annealing. The quartz boats were put in the middle of the furnace through an iron rod. The sample was heated for 4 h at 700 °C. The sample was cooled in the furnace to room temperature [19]. The annealed sample was collected and thus $Mg_xZn_{1-x}Fe_2O_4$ nanoparticles were prepared. Finally, an appropriate amount of Tl_2O_3 was added in $Cu_{0.5}Ba_2Ca_2Cu_3O_{10-\delta}$ and grinded for 1 h. Then $Mg_{0.8}Zn_{0.2}Fe_2O_4$ nanoparticles ($x = 0, 0.5, 1, 1.5$ wt%) were added in CuTl-1223 to make four samples. All samples were pelletized with the help of a hydraulic press at 3.8 ton cm^{-2} pressure. The gold capsules were used for sintering the pellets in a preheated furnace at 860 °C for about ten minutes. The pellets were quenched to room temperature in order to obtain our required $(Mg_{0.8}Zn_{0.2}Fe_2O_4)_x$/CuTl-1223 superconducting matrix.

Results and discussion

The crystalline structure of $Mg_{0.8}Zn_{0.2}Fe_2O_4$ nanoparticles and their phase purity has been determined by using the x-ray diffraction (XRD) analysis. The XRD plot of $Mg_{0.8}Zn_{0.2}Fe_2O_4$ nanoparticles is specified in figure 1. The pattern reveals the spinel structure of $Mg_{0.8}Zn_{0.2}Fe_2O_4$ nanoparticles and the indexed peaks are in perfect accordance with the international center for the diffraction data (ICDD) records. Debye Scherer's formula has been implemented to notice that 29 nm is the nanoparticle size. Exquisitely indexed peaks of $Mg_{0.8}Zn_{0.2}Fe_2O_4$ nanoparticles are (1 1 1), (2 2 0), (3 1 1), (2 2 2), (4 0 0), (4 2 2), (5 1 1), (4 4 0), (6 2 0), (5 3 3) and (6 2 2) are as per pdf files of the ICDD record. The sharpness in the XRD peaks of $Mg_{0.8}Zn_{0.2}Fe_2O_4$ nanoparticles verifies the better crystallinity. The Major development of phase has taken (h k l) value of (3 1 1). Sharpness of peaks represents high crystallinity of $Mg_{0.8}Zn_{0.2}Fe_2O_4$ nanoparticles. The lattice parameter developed is found to be 8.370 Å. The SEM image for 500 nm scale is shown in figure 2. The micrograph specifies that NPs are agglomerated at certain locations due to magnetic inter-particle interaction effects and the particle size is comparable to the one calculated by Sherrer's formula in XRD. The EDX spectrum of $Mg_{0.8}Zn_{0.2}Fe_2O_4$ nanoparticles is shown in figure 3, which confirms the presence of all characteristics elements in the structure. The weight percentages of all present elements are listed in table 1 which shows that there is no impurity in the composition of nanoparticles.

The behavior of $Mg_{0.8}Zn_{0.2}Fe_2O_4$ in the presence of applied magnetic field has been observed in the form of MH-loop at $T = 973$ K by using SQUID magnetometer as given in figure 4. The characteristic loop clearly demonstrates the magnetic nature of NPs. These nanoparticles exhibit saturation magnetization of (5.29 emu g^{-1}) and a coercivity of (89.96 Oe) as evident in the inset of figure 4.

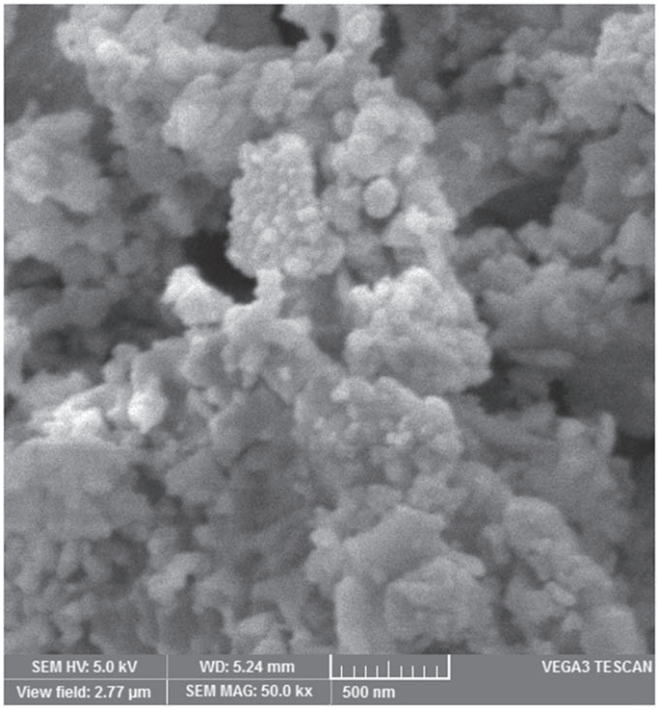

Figure 2. SEM micrographs of $Mg_{0.8}Zn_{0.2}Fe_2O_4$ nanoparticles.

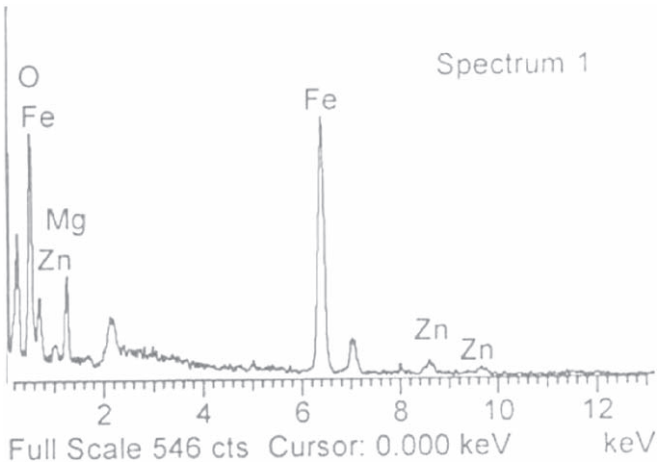

Figure 3. EDX of $Mg_{0.8}Zn_{0.2}Fe_2O_4$ nanoparticles.

Table 1. Mass percentages of elements in $Mg_{0.8}Zn_{0.2}Fe_2O_4$ NP's.

Elements	keV	Weight %	Atomic %
O K	0.2	26.91	52.29
Mg K	1.3	10.30	13.17
Fe K	0.6	57.66	32.10
Zn K	0.7	05.13	02.44
Total		100	100

The XRD patterns of $(Mg_{0.8}Zn_{0.2}Fe_2O_4)_x$/CuTl-1223 superconducting matrix (x = 0, 1.5 wt%) can be seen in the figure 5. MDI Jade computer software has been used for indexation. All the main peaks are indexed according to the tetragonal structure of the host $Cu_{0.5}Tl_{0.5}$–1223 superconducting phase having P4/mmm symmetry. The indexed pattern shows the dominance of CuTl-1223 phase with (0 0 1) plane appearing at

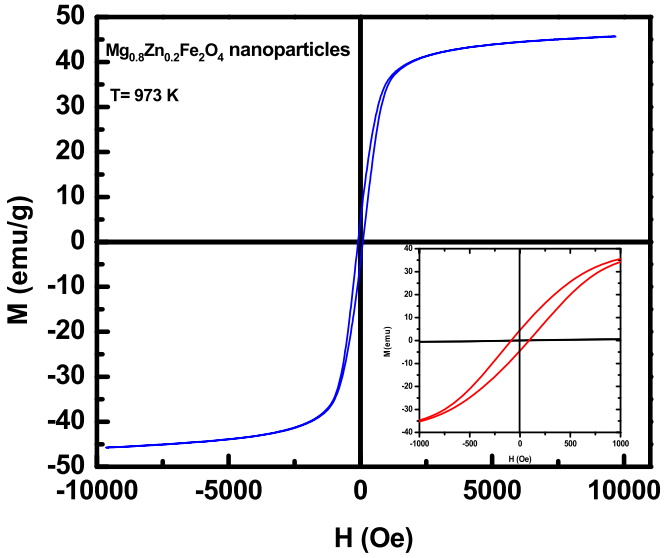

Figure 4. Magnetization curve of $Mg_{0.8}Zn_{0.2}Fe_2O_4$ nanoparticles.

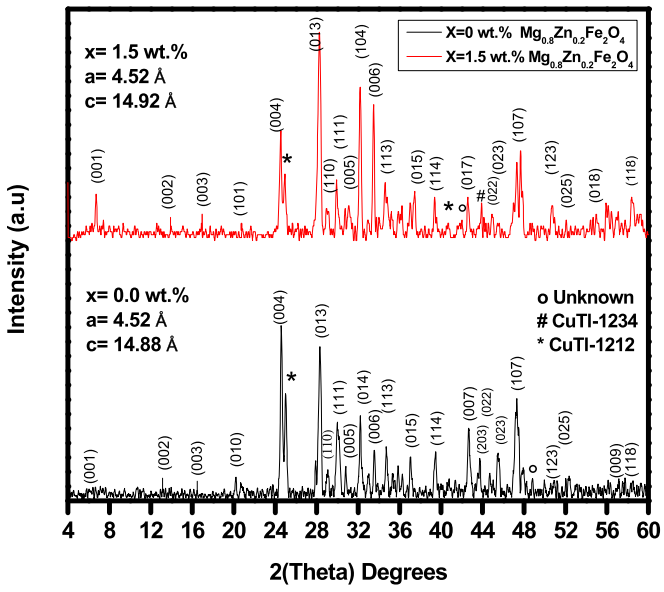

Figure 5. XRD representative patterns of $(Mg_{0.8}Zn_{0.2}Fe_2O_4)_x$/CuTl-1223 (x = 0.0, 1.5 wt%).

$2\theta = 5.98°$. There are some unindexed minor peaks which show the existence of noise and some other superconducting minority phases. The crystalline structure of the host CuTl-1223 superconducting matrix has not been disturbed after addition of $Mg_{0.8}Zn_{0.2}Fe_2O_4$ nanoparticles. This confirms the settlement of inserted $Mg_{0.8}Zn_{0.2}Fe_2O_4$ nanoparticles at the pores and voids existing at the intergranular sites of CuTl-1223 superconducting matrix [20, 21]. Almost all the peaks are very well indexed and there is no major variation in the lattice parameters. It is observed that the tetragonal structure have parameters a = 4.52 Å, c = 4.88 Å, a = 4.52 Å and c = 4.92 Å for x = 0.00 and 1.5 wt% addition of nanoparticles respectively. The presence of the inserted nanoparticles at the grain boundaries play specific role of filling the pores, voids and inter-grain weak-links. A slight variation in lattice parameter may be due to the stresses and strains produced by the added nanoparticles at inter-crystallite sites. The percentages of the impurities or some other miner superconducting phases almost remain the same which may be due to the impurities existing in the initial compounds used during the synthesis process.

Resistivity versus temperature measurements of $(Mg_{0.8}Zn_{0.2}Fe_2O_4)_x$/CuTl-1223 superconducting matrix with various amount of nanoparticles concentrations such as (x = 0, 0.5, 1.0 and 1.5 wt%) are shown in figure 6. The variation in the values of transition temperature $T_c(R = 0)$ for pure superconducting sample and other

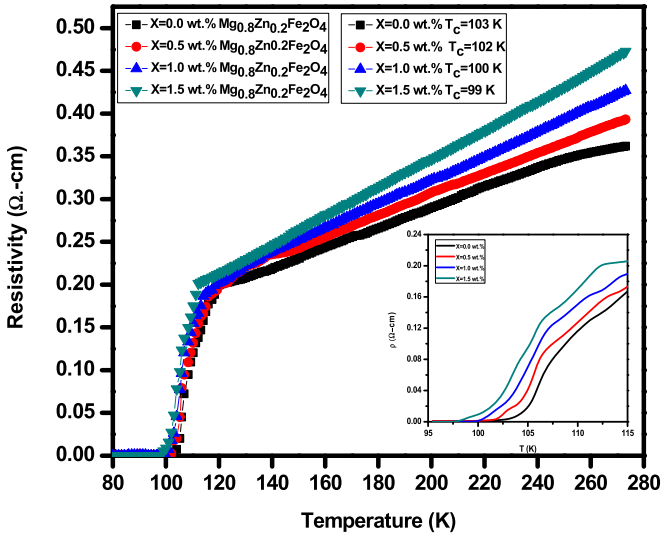

Figure 6. Temperature dependent resistivity measurements of $(Mg_{0.8}Zn_{0.2}Fe_2O_4)_x$/CuTl-1223 composites with (x = 0, 0.5, 1 and 1.5 wt%).

samples with addition of different nanoparticles concentrations in CuTl-1223 matrix is specified in the figure 6. The $T_c(R = 0)$ obtained for pure CuTl-1223 phase is found to be 103 K. The $T_c(R = 0)$ for x = 0.5, 1.00 and 1,5 wt% additions of the nanoparticles in superconducting matrix has values 103 K, 100 K and 99 K respectively. It shows suppression in critical parameters value with the inclusion of magnetic $Mg_{0.8}Zn_{0.2}Fe_2O_4$ nanoparticles. There suppression in T_c values with increase in the concentration of added nanoparticles may be due to the scattering of charge carriers at the grain boundaries because of magnetic natured $Mg_{0.8}Zn_{0.2}Fe_2O_4$ nanoparticles, also, the agglomeration of added nanoparticles and certain inter-granular sites may cause the deterioration of the samples and their superconducting parameters. In high temperature superconductors, there is a resistive broadening observed due to characteristic values of two critical temperatures, one is called T_c^{Onset} (K) which indicate the formation of cooper electron pairs and the other is $T_c(R = 0)$ at which the material enters into bulk superconducting region. The T_c^{Onset} (K) have dependency on electronic characteristics of the material, and, $T_c(R = 0)$ gets influenced by the microstructure of the material and charge carrier concentration in the conducting CuO_2 planes. The materials having weak inter-grain connectivity and higher fraction of voids tends to have lower $T_c(R = 0)$. The suppression in the $T_c(R = 0)$ is not surprising due to the ability of the magnetic nanoparticles to reduce superconductivity. Reduction is critical temperature may be attributed to trapping of free charge carriers and pair breaking at the grain boundaries due to the ferromagnetic nature of $Mg_{0.8}Zn_{0.2}Fe_2O_4$ nanoparticles [22, 23]. The normal state resistivity for all the samples have shown systematic metallic behavior which shows majority of the pores and voids have been successfully filled by the nanoparticles addition. The activation energy of CuTl-1223 phase and their composites can be found by using Arrhenius law given by the equation; $\rho = \rho_o e^{-Uo/k_B T}$. The value ρ_0 is called resistivity, U_0 is called activation energy and K_B is the Boltzmann constant given in the relation. The region very close to $T_c(R = 0)$ have been used to calculate the activation energy U_0. The Arrhenius plots for all $(Mg_{0.8}Zn_{0.2}Fe_2O_4)_x$/CuTl-1223 superconducting composite samples with x = 0, 0.5, 1 and 1.5 wt% concentrations have been shown in figure 7. The activation energy U_0 has been calculated by fitting of the linear part of the Arrhenius plots in the low T_c region. It is evident from the figure that U_0 is decreasing with the increasing concentration of magnetic $Mg_{0.8}Zn_{0.2}Fe_2O_4$ nanoparticles which may be associated with the presence of magnetic nanoparticles at intergranular regions which cause charge carrier scattering and energy dissipation in their transport and ultimately it cause the resistive broadening. Reduction in activation energy U_0 value is also evident for weal flux pinning ability of the resulting composite superconducting samples.

FTIR is a delicate measurement technique for detection of trace amount of functional groups and impurities within the material. Spectra of $(Mg_{0.8}Zn_{0.2}Fe_2O_4)_x$/CuTl-1223 superconducting composite samples with x = 0, 0.5, 1 and 1.5 wt% concentrations have been observed in the far-infrared range of wavenumber (cm^{-1}) as shown in figure 8. The bands till the wave number 450 cm^{-1} are associated with the apical oxygen atoms (O_A). Above this value the bands till 600 cm^{-1} are associated with the planer CuO_2 oxygen atoms and the wavenumber range 670–700 cm^{-1} depicts the O_δ oxygen atom modes which are found in charge reservoir layer [24, 25]. Apical oxygen modes are observed around 456 cm^{-1} and 510 cm^{-1}. The planner oxygen mode is observed at 561 cm^{-1} in all of the $(Mg_{0.8}Zn_{0.2}Fe_2O_4)_x$/CuTl-1223 composite samples. The position of this mode is not altered with

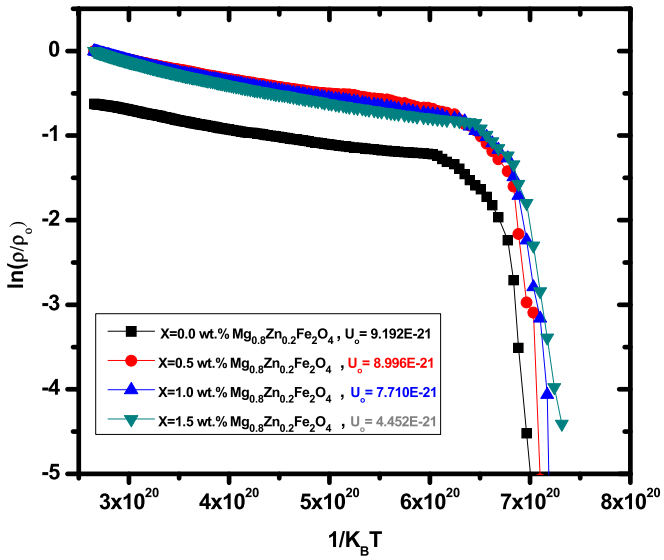

Figure 7. Activation energy plots of $(Mg_{0.8}Zn_{0.2}Fe_2O_4)_x$/CuTl-1223 composites with (x = 0, 0.5, 1 and 1.5 wt%).

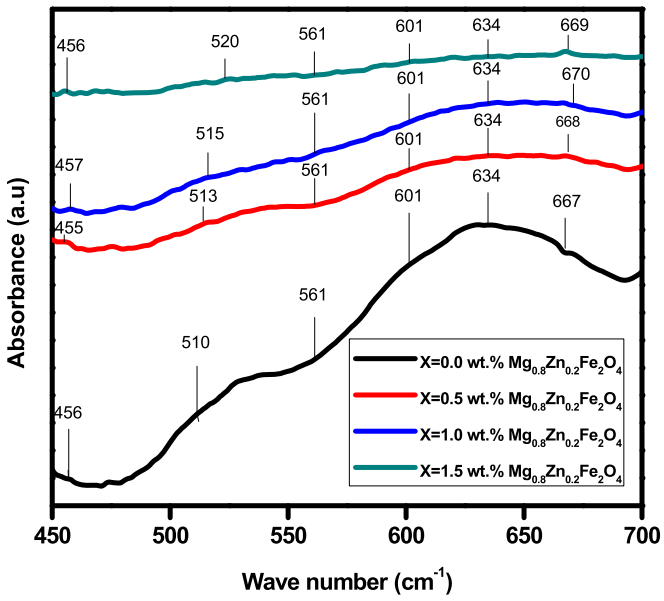

Figure 8. FTIR plots of $(Mg_{0.8}Zn_{0.2}Fe_2O_4)_x$/CuTl-1223 composites with (x = 0, 0.5, 1 and 1.5 wt%).

addition of different concentrations of $(Mg_{0.8}Zn_{0.2}Fe_2O_4)$ nanoparticles. Likewise, no major change has been observed in the planner as well as O_δ oxygen atoms, which is a kind of confirmation that the unit cell structure of the host composite superconducting matrix remains unaltered after the inclusion of different concentrations of magnetic $(Mg_{0.8}Zn_{0.2}Fe_2O_4)$ nanoparticles. A slight variation in the apical oxygen mode may be due to stresses and strains produced by the nanoparticles at the grain boundaries. The FTIR results give an indirect evidence for the existence of the nanoparticles at inter-crystallite sites.

Conclusion

The influences of Magnesium Zinc Ferrite $(Mg_{0.8}Zn_{0.2}Fe_2O_4)$ nanoparticles addition in superconducting CuTl-1223 phase have been investigated. We have synthesized a series of superconducting $(Mg_{0.8}Zn_{0.2}Fe_2O_4)_x$/CuTl-1223 composite samples by using characteristic solid state reaction method for various concentrations of magnetic nanoparticle additions such as (x = 0, 0.5, 1.0, and 1.5 wt%) with the confirmation of their reproducibility. The inserted Magnesium Zinc Ferrite $(Mg_{0.8}Zn_{0.2}Fe_2O_4)$ particles had

spinel structure, ferromagnetic nature as confirmed by the XRD analysis and MH loop measurements. The size of the nanoparticles was found to be 29 nm with a coercivity value of (89.96 Oe and saturation magnetization 5.29 emu g^{-1}. SEM images specify that the nanoparticle are almost spherical in shape and agglomerated by magnetic interactions. The presence of all necessary elements in the composition was confirmed by the EDX plot. It has been revealed that the addition of the inserted $Mg_{0.8}Zn_{0.2}Fe_2O_4$ nanoparticles do not alter the original tetragonal structure of the resulting $(Mg_{0.8}Zn_{0.2}Fe_2O_4)_x$/CuTl-1223 composite superconducting samples. There is no variation in the XRD pattern after the insertion of magnetic nanoparticles. This observation specifies the presence of the added nanoparticles at the pores and voids available at inter-crystallite regions. FTIR plots show no major shifting in oxygen modes for various additions of magnetic nanoparticles, which confirm the presence of nanoparticles at inter-granular regions. The critical temperature of the superconducting $(Mg_{0.8}Zn_{0.2}Fe_2O_4)_x$/CuTl-1223 composites was observed to get reduced with the increasing concentrations of the added magnetic nanoparticles and the activation energy U_o was also seen to get suppressed in direct relation with increasing nanoparticles concentration. The reason behind the reduced critical parameters and activation energy may be the ability of the magnetic nanoparticles to scatter the charge carriers at the grain boundaries and generate additional energy dissipation for their transport, also the pair breaking mechanism and trapping of carries at the inter-granular regions cause reduction in critical temperature. Suppression in U_o is directly linked with the flux pinning capability, so, the superconducting $(Mg_{0.8}Zn_{0.2}Fe_2O_4)_x$/CuTl-1223 composites illustrate reduced flux pinning with increasing magnetic nanoparticles content.

Acknowledgments

We are highly thankful to Dr Nawazish A Khan for providing the characterization facilities at Material Science Laboratory, Department of Physics (QAU) Islamabad and Dr Muhammad Mumtaz for supporting the synthesis process at Material Research Laboratory, Department of Physics (IIU) Islamabad.

ORCID iDs

Irfan Qasim https://orcid.org/0000-0003-3651-3863
Qurat ul Ain Javed https://orcid.org/0000-0001-8230-1381
Muhammad Mumtaz https://orcid.org/0000-0002-5437-6244

References

[1] Xu Y, Hu A, Xu C, Sakai N, Hirabayashi I and Izumi M 2008 Effect of ZrO_2 and ZnO nanoparticles inclusions on superconductive properties of the melt-processed $GdBa_2Cu_3O_{7-\delta}$ bulk superconductor *Physica C: Superconductivity* **468** 1363–5
[2] Ihara H *et al* 2000 Mechanism of Tc enhancement in $Cu_{1-x}Tl_x$-1234 and -1223 system with Tc > 130 K *Physica.* C **48** 341–8
[3] Hafiz M and Abd-Shukor R 2014 Effect of nanosized $Co_{0.5}Ni_{0.5}Fe_2O_4$ on the transport critical current density of $Bi_{1.6}Pb_{0.4}Sr_2Ca_2Cu_3O_{10}$ superconductor *AIP Conf. Proc.* **1614** 30
[4] Awad R, Aly A I A, Mohammed N H, Isber S, Motaweh H A and Bakeer D E-S 2014 Effect of Fe_2O_3 nano-oxide addition on the superconducting properties of the (Bi, Pb)-2223 phase *J. Supercond. Novel Magn.* **27** 143–53
[5] Abbasi H, Taghipour J and Sedghi H 2010 Superconducting and transport properties of (Bi–Pb)–Sr–Ca–Cu–O with Cr_2O_3 additions *J. Alloys Comp.* **494** 305–8
[6] Jha A K and Khare N 2009 Strongly enhanced pinning force density in YBCO-$BaTiO_3$ nanocomposite superconductor' *Physica C: Superconductivity* **469** 810–3
[7] Tsai C F, Huang J, Lee J H, Khatkhatay F, Chen L, Chen A, Su Q and Wang H 2015 Tunable 'flux pinning landscapes achieved by functional ferromagnetic Fe_2O_3:CeO_2 vertically aligned nanocomposites in $YBa_2Cu_3O_{7-\delta}$ thin films *Physica C: Superconductivity* **510** 13–20
[8] Mohammed N H, Abou-Aly A I, Ibrahim I H, Awad R and Rekaby M 2011 Effect of Nano-Oxides Addition on the Mechanical Properties of $(Cu_{0.5}Tl_{0.5})$-1223 Phase *J. Supercond. Novel Magn.* **24** 1463–72
[9] Mohammed N H, Abou-Aly A I, Awad R, Ibrahim I H, Roumié M and Rekaby M 2013 Mechanical and Electrical Properties of $(Cu_{0.5}Tl_{0.5})$-1223 Phase Added with Nano-Fe_2O_3 *J. Low Temp. Phys. Vol* **172** 234–55
[10] Mumtaz S, Naeem K, Nadeem F, Naeem and Abdul Jabbar Y R 2013 Zheng, Nawazish A. Khan and M. Imran. 'Study of nano-sized $(ZnFe_2O_4)_y$ nanoparticles/CuTl-1223 superconductor composites' *J. Solid State Sci.* **22** 21–6
[11] Suazlina M A, Yusainee S Y S and Azhan H 2014 Abd. Shukor, and R. Mustaqim, 'The effects of nanoparticle addition in Bi-2212 superconductors *Journal Teknologi (Sciences and Engineering)* **69** 49–52
[12] Mellekh A, Zouaoui M, Ben Azzouz F, Annabi M and Ben Salem M 2006 'Nano- Al_2O_3 particle addition effects on Y $Ba_2Cu_3O_y$ superconducting properties' *Solid State Commun.* **140** 318
[13] Ghattas A, Azzouz F B, Annabi M, Zouaoui M and Salem M B 2008 Pinning mechanism in (Bi, Pb)−2223 polycrystalline samples prepared with Al_2O_3 nano-particles' *J. Phys.: Conf. Ser.* **97** 012175
[14] Xu C, Hu A, Sakai N, Izumi M and Hirabsyashi I 2005 Effect of BaO_2 and fine $Gd_2BaCuO_{7-\delta}$ addition on the superconducting properties of air-processed $GdBa_2Cu_3O_{7-\delta}$ *Supercond. Sci. Technol.* **18** 229
[15] Zouaoui M, Ghattas A, Annabi M, Azzouz F B and Salem M B 2009 Magneto-resistance analysis of nanometer $A1_2O_3$ added Bi-2223 polycrystalline superconductors' *J. Phys.: Conf. Ser.* **150** 052292

[16] Dadras S, liu Y, Chai Y S, Daadmehr V and Kim K H 2009 Increase of critical current density with doping carbon nano-tubes in $YBa_2Cu_3O_{7-\delta}$ *Physica C: Superconductivity* **469** 55–9
[17] Qurat-ul-ain and Khan N A 2014 Fluctuation induced conductivity analysis of Mn doped $Cu_{0.5}Tl_{0.5}Ba_2Ca_2Cu_{3-x}Mn_xO_{10-\delta}$ ($x = 0$, 0.1, 0.15) superconductors *J. Appl. Phys.* **116** 103904
[18] Qasim I, Rehman M W, Mumtaz M, Hussain G, Nadeem K and Khan N A 2015 Role of anti-ferromagnetic Cr nanoparticles in CuTl-1223 superconducting matrix *J. Alloys Comp.* **649** 320–326
[19] Rahman S, Nadeem K, Rehman A, Mumtaz M, Naeem S and Papst I L 2013 Structural and Magnetic Properties of ZnMg-Ferrite Nanoparticles Prepared Using the Co-Precipitation Method *J. Ceram. Int.* **39** 5235–9
[20] Jabbar A, Qasim I, Khan S A, Nadeem K, Waqee-ur-Rehman M, Mumtaz M and Zeb F 2015 Highly coercive cobalt ferrite nanoparticles-CuTl-1223 superconductor composites *J. Magn. Mag. Mater.* **377** 6–11
[21] Jabbar A, Qasim I, Waqee-ur-Rehman M, Zaman M, Nadeem K and Mumtaz M 2015 Structural and superconducting properties of $(Al_2O_3)y$/CuTl-1223 composites *J. Electron. Mater.* **44** 110–6
[22] Kulkarni A D, de Wette F W, Prade J, Schroder U and Kress W 1990 Lattice dynamics of high-T_c superconductors: optical modes of the thallium-based compounds *Phys. Rev.* B **41** 6409–17
[23] Mumtaz M, Khan N A and Khan E U 2010 Growth of $Cu_{0.5}Tl_{0.5}Ba_2Ca_3Cu_{4-y}Zn_yO_{12-\delta}$ ($y = 0$, 1, 1.5, 2, 2.5) superconductor with optimum carriers *Physica C: Superconductivity* **470** 434
[24] Knobe M, Nunes W C, Winnischofer H, Rocha T C R, Socolovsky L M, Mayorga C L and Zanchet D 2007 Effects of magnetic inter-particle coupling on the blocking temperature of ferromagnetic nanoparticle arrays' *J. Non-Cryst. Solids* **353** 743–7
[25] Khan N A, shah S Q A and Mahmood A 2015 Synthesis and Para-conductivity of $(Tl_{1-x}Ti_x)Ba_2Ca_2Cu_3O_y$ ($x = 0$, 0.2, 0.4, 0.6, 0.8) Superconductors *J. Supercond. Novel Magn.* **182** 1–2